A method to investigate mid and high-frequency vibration energy transfer paths using the irrotational intensity

Jamal Takhchi[a,c,d], Morvan Ouisse[a], Emeline Sadoulet-Reboul[b], Noureddine Bouhaddi[b], Laurent Gagliardini[c], Frédéric Bornet[c], Léon Gavric[c], Faouzi Lakrad[d]

[a] *SUPMICROTECH, Université de Franche Comté, CNRS, Institut FEMTO-ST, F-25000, Besançon, France*
[b] *Université de Franche Comté, CNRS, Institut FEMTO-ST, F-25000, Besançon, France*
[c] *STELLANTIS, Research and Development Division, Technical Center of Belchamp, Voujeaucourt, 25420, France*
[d] *LERDS, FSAC, Hassan II University , Casablanca, 20000, Morocco*

Abstract

Structural intensity fields provide a clear understanding of the noise, vibration and harshness (NVH) behavior of complex structures by showing the vibration energy flow between zones of excitation and dissipation. The use of models with fine meshes for automotive structures has allowed structural intensity calculations to be performed at high frequencies. However, fields are difficult to understand at medium and high frequencies: the intensity field has a vortical character that hides the vibration energy flow in these frequency ranges. In this work, a methodology is presented to filter out vortices in the structural intensity field. The approach uses the Hodge-Helmholtz decomposition: the structural intensity field is decomposed into rotational, irrotational, and harmonic components. Among them, only the irrotational component is needed to describe the path of energy flow from sources to sinks. The proposed methodology involves calculating the dynamic response and solving a diffusion equation similar to the thermal conduction equation to obtain the irrotational field of interest. Plate examples are used to illustrate the efficiency of the method, which provides a better understanding of the mid- and high-frequency energy transmission paths.

1. Introduction

In the automotive industry, using energy-based methods to predict the mid- and high-frequency vibration behavior of complex structures is more efficient than conventional methods (modal analysis and frequency responses). Standard structural dynamics techniques have challenges understanding behavior at high frequencies due to increasing modal overlap. In addition, the vibration behavior changes considerably from one frequency to another, and the dynamic response is highly affected by small changes in the structural properties. Fortunately, it is expected—for long-time experimental observations—that energy analysis can provide a robust understanding of vibration propagation at least at high frequencies.

Statistical energy analysis (SEA) is a method developed to provide an approximate model of the behavior of a built-up structure at high frequencies [1]. The technique is efficient at very high frequencies and requires a high modal overlap [2]. In the SEA method, large structures are divided into smaller subsystems. A modal density is then estimated for each subsystem so that the number of modes in a given frequency band can be determined. SEA assumes that the flow of energy between two subsystems is proportional to the difference in their averaged modal energies. This assumption has many drawbacks, especially for heterogeneous structures in the mid-frequency range where global and local modes may coexist. Determining the coupling loss factors then becomes a real challenge. Researchers have devoted significant attention to deriving the coupling loss factor from impedance and transmission efficiency information [3–5], highlighting the inability of standard SEA to model local behaviors within systems or in their connection's vicinity [6–11].

Therefore, other methods have been investigated to predict the dynamic response of structures. Energy finite element analysis or power flow finite element analysis (PFFEM) dates back to the 1970s. The technique uses the same quantities (energy density and energy flow) as SEA. The approach is based on a simplified equation similar to that of steady-state heat conduction, thanks to the acoustic temperature concept developed in early SEA research [1]. The method has been applied with significant success to one-dimensional structures. Nefske and Sung [12] developed and implemented the method numerically for beams using the finite element to solve the conduction equation. They compared their energy solution to that of SEA and to the exact solution. The PFFEM correctly predicts the average frequency

and spatial response of the beam. It shows the fluctuation of the average response along the beam (the local behavior), which is not provided by the SEA method. The method becomes more efficient as the frequency increases. Bouthier and Bernhard [13] deduced the same equation for plates. The approach was then applied to a single plate. The structural responses of the considered examples (lightly damped plates) were accurately obtained. However, the method is likely to encounter several difficulties for highly damped plates. In this case, the direct field is likely to represent a significant part of the structural response, and the mathematical form of the direct field predicted by the steady-state heat conduction equation is not consistent with the known exact results [14].

Structural intensity was introduced in the 1970s to extend the notion of acoustic intensity. It corresponds to the density of energy flow carried by vibration waves. The spatial distribution of the structural intensity in a given structure provides information on the energy transmission paths and the positions of energy sources and sinks. The first studies concerning structural intensity dealt with the theoretical development and implementation of measurement methods [15, 16]. Initially, the structural intensity field was assessed using contact methods, such as accelerometers. The internal forces were estimated numerically by the finite differences. The main limitation of this approach was the modification of the vibration behavior of the system due to the additional mass of the accelerometers. Later, noncontact methods that do not add mass to the measured structure were used to detect surface motions, such as acoustic holography [17], laser Doppler vibrometry [18], holographic interferometry [19] and electron speckle interferometry [20]. Recently, a new technique has been developed to measure the structural intensity field in a plate [21]. This technique allows the structural intensity field to be reconstructed from the measured data (plate displacements) using just a single moving sensor. However, the experimental characterization of the structural intensity field is still inherently inaccurate. The spatial derivation operator used to calculate the internal forces from displacements amplifies the noise of the measurements.

Structural intensity analysis using the finite element method was formulated by Hambric [22], and Gavric [23]. This approach has been successfully used to numerically investigate major vibration transmission paths in structures at low frequencies [23–34]. The use of finite element models with finer meshes for automotive structures allows this approach to be extended to medium and high frequencies. However, understanding the structural inten-

sity field becomes more difficult as the frequency increases. The field presents a vortex behavior that masks the energy flow from the source to the dissipation zones in the structure. Various studies have been conducted to eliminate this vortex behavior of the structural intensity field. The structural intensity vector field is composed of a rotational and an irrotational part [35]. The rotational intensity is responsible for the vortices of the structural intensity field showing conservative energy circulation. On the other hand, the irrotational intensity is related to how energy flows from the sources to the sinks. A direct application was proposed for plates [36] that uses the irrotational part of the acoustic intensity field to identify and locate energy sources in a plate. A method to evaluate the irrotational intensity has been proposed. It uses a calculation in the wavenumber domain from a known radiated intensity field over the whole space. Later, a method that computes the irrotational part from measurement data was developed [37]. The approach is called test functional series (TFS). It was used to determine the vibration sources and sinks in a single plate.

In many studies, the irrotational intensity was mainly used to identify the sources and sinks of vibration energy. However, the methods used to extract this component are not practical in an industrial context, as they are based on representations in infinite domains and do not consider the boundary conditions of the intensity field. The purpose of this paper is twofold: first, a new and rigorous technique is proposed to extract the irrotational component of the structural intensity field in the framework of the finite element method. Second, we show an academic application of this technique : the irrotational intensity allows a better understanding of the transfer paths of structures without the masking effect of energy loops related to the rotational intensity. These two steps open the way to industrial applications with higher structural complexity. This paper is organized as follows: definitions and equations related to structural intensity are presented in section 2. In section 3, the theoretical concepts and the methodology for rotational intensity filtering are discussed. Section 4 shows the calculation of the structural intensity and the associated irrotational intensity on a simply supported plate. Section 5 presents the analysis of the propagation of vibration energy in a rectangular plate structure using the irrotational intensity field.

2. Structural intensity

The instantaneous structural intensity is a time-dependent vector quantity that represents the variation in the energy density in an infinitesimal volume. It is mathematically defined at a point M of the structure and at time t as:

$$\mathbf{\Pi}(M,t) = -\boldsymbol{\sigma}(M,t)\mathbf{v}(M,t), \tag{1}$$

where $\boldsymbol{\sigma}(M,t)$ and $\mathbf{v}(M,t)$ stand for the stress tensor and the velocity vector, respectively.

In the case of steady-state harmonic vibrations, for a given frequency, the time average of the structural intensity over a period represents the net energy flow in the structure, and it can be expressed as:

$$\mathbf{I}(M,\omega) = -\frac{1}{2}\Re(\boldsymbol{\sigma}(M,\omega)\mathbf{v}^*(M,\omega)), \tag{2}$$

where $\boldsymbol{\sigma}(M,\omega)$ and $\mathbf{v}(M,\omega)$ are the stress tensor and the velocity vector at point M and frequency ω, respectively, and $\Re$ stands for the real part of a complex number. The symbol * denotes the complex conjugate operator. In the following, M and ω are omitted to simplify the notation.

The time average of the structural intensity in the case of a flat thin plate in the (x,y) plane is expressed as [38]:

$$\begin{cases} I_x = -\frac{\omega}{2}\Im(N_x u^* + N_{xy} v^* + Q_x w^* + M_x \theta_y^* - M_{xy}\theta_x^*) \\ \\ I_y = -\frac{\omega}{2}\Im(N_y v^* + N_{xy} u^* + Q_y w^* - M_y \theta_x^* + M_{xy}\theta_y^*) \end{cases} \tag{3}$$

where I_x and I_y represent the components of the structural intensity field along the x and y directions, respectively. N_x, N_y and N_{xy} are the complex membrane forces. M_x, M_y and M_{xy} are the complex bending and torsional moments. Q_x and Q_y are the complex shear forces. The displacement components of the plate are denoted by u, v and w, and the angular displacements are denoted by θ_x and θ_y. $\Im$ stands for the imaginary part of a complex number.

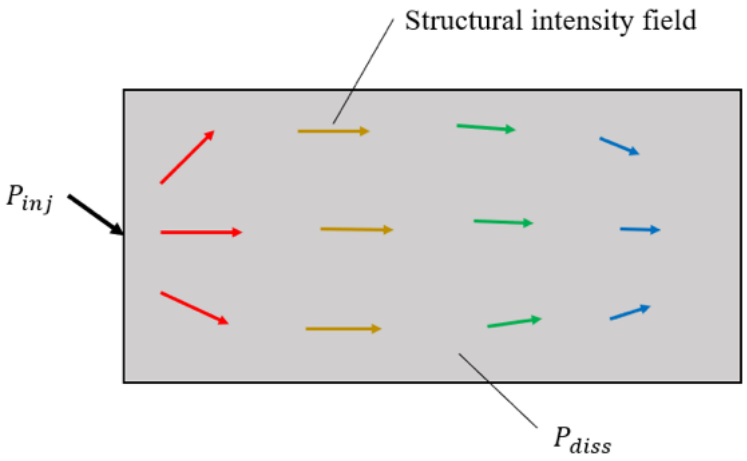

Fig. 1. Sample chart of the structural intensity field

Fig. 1 shows a typical vibration energy flow pattern. The power P_{inj} is injected at a specific location via dynamic loading. The vibration energy flows through the structure along several flow paths represented by arrows whose length and color represent the magnitude of the energy flow. As the energy travels through the structure, it is dissipated by material damping and other dissipation phenomena. This is illustrated by the arrow lengths becoming shorter. The dissipated power is refered to as P_{diss}.

In this study, the input power is injected through a single point of the structure and is written as,

$$P_{inj} = \frac{1}{2}\Re(\mathbf{F}.\mathbf{v}_{in}^{*}), \tag{4}$$

where $\mathbf{F}$ is the excitation force vector applied to the structure, and $\mathbf{v_{in}}$ is the velocity vector at the excitation point. Since energy quantities are proportional to the input power, most of the results will be normalized to a unit input power.

When the dissipation is due to structural (hysteretic) damping, the power dissipated per unit area within a structure vibrating in the harmonic regime at frequency ω is usually expressed as [39]:

$$P_{diss} = 2\eta\omega E_d, \tag{5}$$

where η denotes the implicitly frequency-dependent structural damping loss factor and E_d stands for the strain energy density. Without loss of

generality, only structural damping is considered in the following.

The local energy balance in steady-state harmonic vibrations of an elastic medium is equivalent to the variation in the structural intensity field [39]:

$$\boldsymbol{\nabla}.\mathbf{I} = P_{inj} - P_{diss}. \tag{6}$$

The structural intensity divergence can then be estimated using the power injected and the power dissipated per unit area through the structure.

The power flow through a cross-section S can be calculated using the following Formula:

$$P_f = \iint_S \mathbf{I}.\mathbf{ds} \tag{7}$$

In the case of structure assemblies, the power flow from substructure i to substructure j is expressed in terms of structural intensity by the following formula:

$$P_{i\to j} = \iint_{S_b} \mathbf{I}.\mathbf{ds} \tag{8}$$

where S_b is the common section shared by the two substructures.

3. IRROTATIONAL INTENSITY FIELD CALCULATION

3.1. Helmholtz-Hodge theorem

The Helmholtz-Hodge theorem states that any vector field $\mathbf{u}$ can be decomposed into the sum of three components: an irrotational component $\mathbf{u}_\psi$ derived from the gradient of a scalar potential ψ, a rotational component $\mathbf{u}_{\boldsymbol{\phi}}$ resulting from the curl of a vector potential $\boldsymbol{\phi}$ and a harmonic part $\mathbf{u}_h$, that cannot be included in either of the two previous components, which is both irrotational and rotational at the same time [40]:

$$\mathbf{u} = \mathbf{u}_\psi + \mathbf{u}_{\boldsymbol{\phi}} + \mathbf{u}_h. \tag{9}$$

Following this theorem, the structural intensity field $\mathbf{I}$ can be decomposed into a rotational intensity $\mathbf{I}_r$, an irrotational intensity $\mathbf{I}_{ir}$, and a harmonic part $\mathbf{h}$:

$$\mathbf{I} = \mathbf{I}_r + \mathbf{I}_{ir} + \mathbf{h}. \tag{10}$$

3.2. Rotational intensity

The rotational intensity field is derived from a potential vector $\mathbf{A}$:

$$\mathbf{I}_r = \boldsymbol{\nabla} \wedge \mathbf{A}. \tag{11}$$

This component is responsible for the complexity of the structural intensity field. It leads to vortices due to interference between propagative waves [35], but it does not provide any information about energy transfer.

The local energy balance associated with the rotational intensity is zero at any point of the structure as the divergence of the curl is zero:

$$\boldsymbol{\nabla}.\mathbf{I}_r = \boldsymbol{\nabla}.(\boldsymbol{\nabla} \wedge \mathbf{A}) = 0. \tag{12}$$

Similarly, the global balance of the rotational intensity is zero for any volume V bounded by a closed surface S. It can be computed as an integral over a surface or a volume using the divergence theorem as follows:

$$\begin{aligned} \oiint_S \mathbf{I}_r.\mathbf{n}\, ds &= \oiint_S \boldsymbol{\nabla} \wedge \mathbf{A}\, ds \\ &= \iiint_V \boldsymbol{\nabla}.(\boldsymbol{\nabla} \wedge \mathbf{A}) dv \\ &= 0. \end{aligned}$$

Thus, the rotational intensity cannot start or end on a source or a sink of energy because of its rotational nature. It either forms closed loops or starts and ends at infinity. It does not affect the quantitative assessment of the transfer of vibration energy.

3.3. Irrotational intensity and heat conduction equation

The irrotational intensity is derived from a scalar potential ψ:

$$\mathbf{I}_{ir} = -\boldsymbol{\nabla}\psi. \tag{13}$$

It describes the transport of energy from injected power sources to dissipative areas [35].

Using the Helmholtz-Hodge decomposition, the local power balance is rewritten as :

$$\begin{aligned}\boldsymbol{\nabla}.\mathbf{I} &= \boldsymbol{\nabla}.(\mathbf{I}_r + \mathbf{I}_{ir} + \mathbf{h}) \\ &= \boldsymbol{\nabla}.(\boldsymbol{\nabla} \wedge \mathbf{A}) + \boldsymbol{\nabla}.(-\boldsymbol{\nabla}\psi) + \boldsymbol{\nabla}.\mathbf{h}.\end{aligned}$$

The divergence of the rotational intensity and of the harmonic component is zero. Thus,

$$\boldsymbol{\nabla}.\mathbf{I} = -\boldsymbol{\nabla}.\boldsymbol{\nabla}\psi. \tag{14}$$

The structural intensity $\mathbf{I}$ and the irrotational intensity $\boldsymbol{\nabla}\psi$ share the same divergence.

The flow of vibration energy through a closed surface S can be rewritten using Eq.(9) as:

$$\begin{aligned}\oiint_S \mathbf{I}.\mathbf{n}\, ds &= \iiint_V \boldsymbol{\nabla}.\mathbf{I}\, dv \\ &= \iiint_V \boldsymbol{\nabla}.(\mathbf{I}_r + \mathbf{I}_{ir} + \mathbf{h})\, dv \\ &= \iiint_V \boldsymbol{\nabla}.\mathbf{I}_r\, dv + \iiint_V \boldsymbol{\nabla}.\mathbf{I}_{ir}\, dv + \iiint_V \boldsymbol{\nabla}.\mathbf{h}\, dv \\ &= \iiint_V \boldsymbol{\nabla}.\mathbf{I}_{ir}\, dv.\end{aligned}$$

Thus,

$$\oiint_S \mathbf{I}.\mathbf{n}\, ds = \oiint_S \mathbf{I}_{ir}.\mathbf{n}\, ds = \iiint_V (P_{inj} - P_{diss})\, dv. \tag{15}$$

The energy flow through a closed section of the structure depends only on its irrotational component. Therefore, it is convenient to describe the propagation of vibration energy using only the irrotational intensity.

By combining the local energy balance in steady-state Eq.(6) and Eq.(14), a new equation governing the vibration energy flow is derived. The equation is analogous to the heat conduction equation:

$$-\boldsymbol{\nabla}.\boldsymbol{\nabla}\psi = P_{inj} - P_{diss}. \tag{16}$$

Eq.(16) highlights that the irrotational intensity is directly linked to the energy sources and sinks. To obtain this vector field, Eq.(16) must be solved, in which the potential scalar ψ is the unknown quantity, and its gradient $\boldsymbol{\nabla}\psi$ represents the irrotational intensity field. The right-hand side of the equation is obtained from a dynamic response under harmonic excitation. The dissipated power is obtained using Eq.(5). The injected power is determined from Eq.(4). Practically speaking, the injected power can therefore be considered as a thermal source in the diffusion Eq.(16), which can then be solved with a thermal solver.

3.4. Harmonic field

There are two distinct forms of harmonic fields. The first is specific to the domain topology, and it is at the essence of Hodge's work [40]. The second is due to the choice of boundary conditions for the other components of the decomposition calculation. In general, boundary conditions serve to ensure orthogonality of the various components. Finding the right boundary conditions that ensure this orthogonality often necessitates introducing a third term into the decomposition. The harmonic field, in other words, is a residue of the irrotational and rotational component calculations. For a theoretical and numerical analysis of this field, the reader is invited to refer to the work of Lemoine [41] and Bhatia [42, 43]. For our purpose, the irrotational intensity is the component of interest. In the following section, we will illustrate the boundary conditions to be used to compute this component. The boundary conditions to obtain the rotational intensity are not yet known. We assume here that the harmonic component is part of the rotational component since these two components do not contribute to the flow of vibration energy from a source to the dissipation zones. The intensity field decomposition is then reduced to just two components: rotational and irrotational.

3.5. Boundary conditions

Boundary conditions are required to solve Eq.(16) on the considered domain. We consider a structural problem with no energy transfer to the outside of the structure and no dissipation at the boundary. Therefore, the case of energy free boundaries is considered here. The normal energy flow is zero at such free boundaries, which describes a total reflection of the energy flow. Thus, the boundary conditions are written as

$$\boldsymbol{\nabla}\psi.\mathbf{n} = \frac{\partial\psi}{\partial n} = 0, \tag{17}$$

where $\mathbf{n}$ is the unit vector normal to the considered boundary.

3.6. Power flow decomposition

Same as the structural intensity field, the power flow through a cross-section S can be decomposed into two components: irrotational power flow P_{ir} and rotational power flow P_r. The total power flow represented by the structural intensity can then be rewritten as follows:

$$P_f = P_{ir} + P_r \tag{18}$$

where,

$$P_{ir} = \iint_S \mathbf{I_{ir}}.\mathbf{ds} \tag{19}$$

$$P_r = \iint_S \mathbf{I_r}.\mathbf{ds} \tag{20}$$

3.7. Streamlines for structural intensity field analysis

In fluid mechanics, a streamline is a curve in space whose tangent, at any time, is parallel to the local velocity of the fluid particles. Structural intensity is the flow of vibration energy through a structure. It is characterized by a vector field, known at any point of the structure. Analogously, we can define the streamlines that correspond to the structural intensity field since they provide a better visualization of vibration energy flows.

For the structural intensity field defined at each point by the vector $\mathbf{I}(\mathbf{x}, \mathbf{y}, \mathbf{z})$, the differential equations of the streamlines are expressed as follows:

$$\frac{dx}{I_x} = \frac{dy}{I_y} = \frac{dz}{I_z} \tag{21}$$

3.8. Numerical implementation

First, a structural dynamic response under harmonic excitation is required to determine the right-hand side of Eq.(16). The dissipated power per unit area (P_{diss}) is determined from the strain energy density, while the injected power (P_{inj}) is assessed using the velocity at the excitation point. This forced response can be calculated with the use of any appropriate finite element dynamic solver, and it is worth noting that strain energy densities

and velocities are typically standard outputs provided by most finite element solvers.

Second, the solution of the diffusion Eq.(16) is computed by the finite element method using a thermal solver applied to the same finite element geometry, with the appropriate thermal properties and thermal load. Fig. 2 shows the flowchart of the irrotational intensity calculation.

Practically speaking, all results presented in this paper are obtained using Nastran software. The dynamic response corresponds to a direct frequency response analysis (SOL108) and the thermal response corresponds to a steady state analysis (SOL153), but it is worth noting that any dynamic or thermal solver can be used. The method is set to be applied to industrial structures involving solids, shells and beams. The modeling of the specific industrial connections will be the subject of a future article.

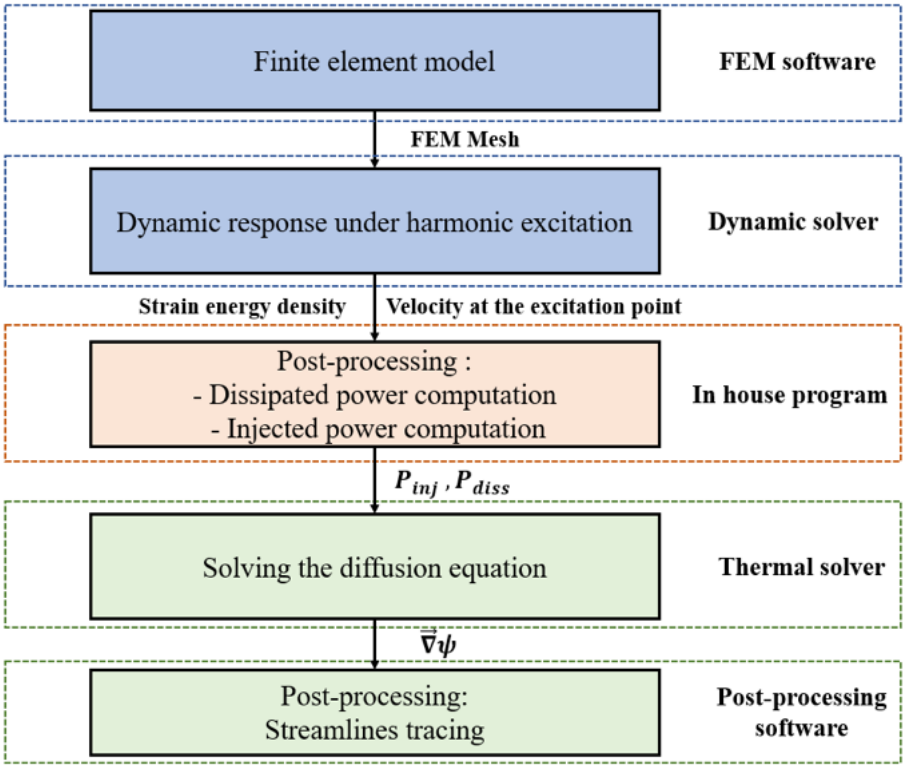

Fig. 2. Scheme of the computational system for the irrotational intensity field

4. POWER FLOW ANALYSIS USING THE IRROTATIONAL INTENSITY FIELD IN A SINGLE PLATE

The model adopted to validate the numerical implementation is a homogeneous flat plate. The plate has the properties shown in Table 1. The square plate (1×1 m^2) is simply supported along its edges and is excited by a harmonic normal force **F** of 1 N at the center, as shown in Fig. 3. A uniform mesh of 50 linear quadrilateral elements (5 dofs per node) along each direction is used for all computations.

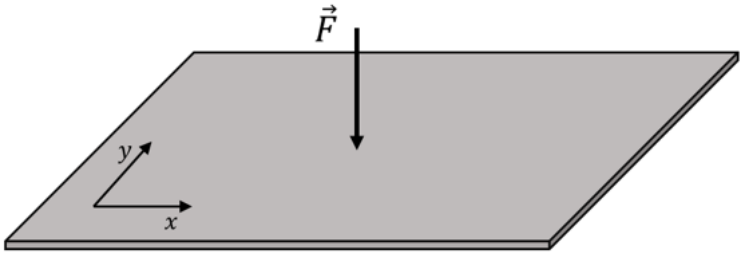

Fig. 3. Plate excited by harmonic force

Length (mm)	1 000
Width (mm)	1 000
Thickness (mm)	1
Elastic modulus (MPa)	210 000
Poisson ratio	0.3
Density (kg/m^3)	7 800
Structural loss factor	1%

Table 1: Plate properties

Fig. 4 shows the structural intensity field and the associated irrotational intensity field at different frequencies for a unit power input. The structural intensity field is calculated using Eq.(3), and the irrotational intensity is assessed by solving Eq.(16). The vector fields are drawn using streamlines, and the color corresponds to the amplitude of the vectors.

At 10 Hz, the structural intensity and the irrotational intensity fields appear to be similar. Indeed, at low frequencies, i.e., below the first structural mode, the dynamic response is quasistatic. No propagation occurs, and a

transmission path does not mean much. Nevertheless, interestingly, in the case of quasistatic stiffness behavior, the rotational intensity component is not present.

At higher frequencies, the structural intensity field presents vortices that mask the energy flow, making it challenging to understand the transfer paths. The number of vortices in the field increases with frequency. On the other hand, the irrotational intensity is smoother and is not perturbed by vortices. The field clearly indicates the position of the source and the isotropic dissipation of energy through the plate due to uniform structural damping. As expected, no energy is transferred to the exterior, so all vectors near the boundaries are parallel to the edges. It may also be noted that in this simple case, the energy flow scheme appears almost frequency independent. Thus, a transfer path—as expected from a practical point of view—makes sense over a broad frequency band.

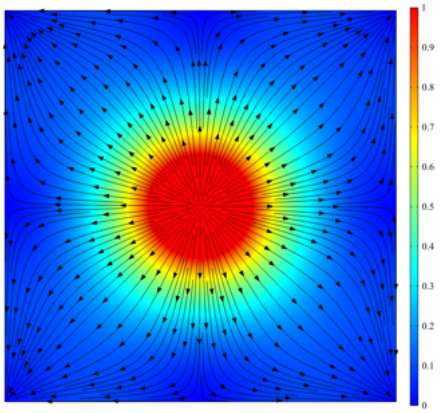

(a) Structural intensity field at 10 Hz

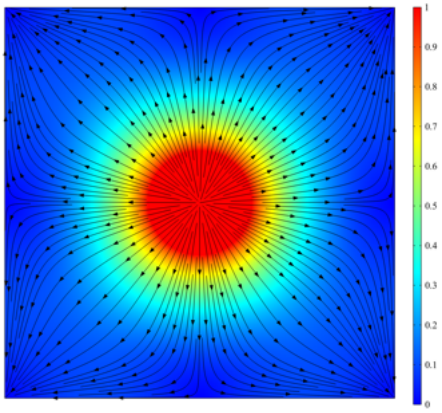

(b) Irrotational intensity field at 10 Hz

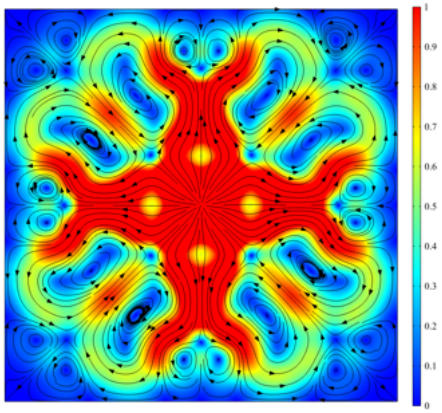

(c) Structural intensity field at 200 Hz

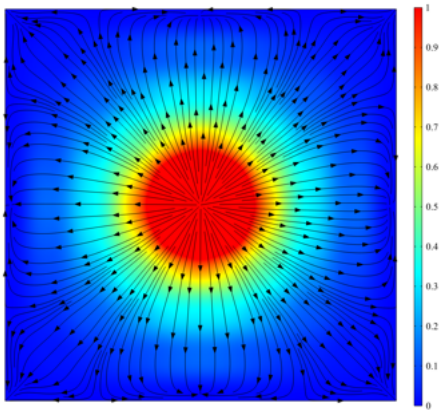

(d) Irrotational intensity field at 200 Hz

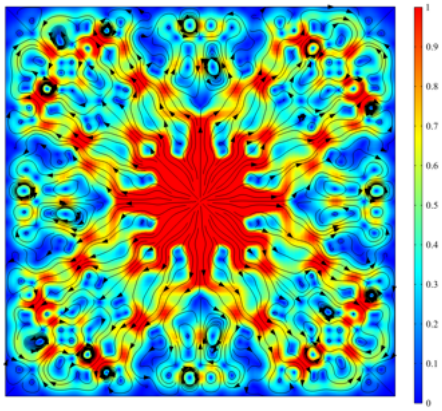

(e) Structural intensity field at 1000 Hz

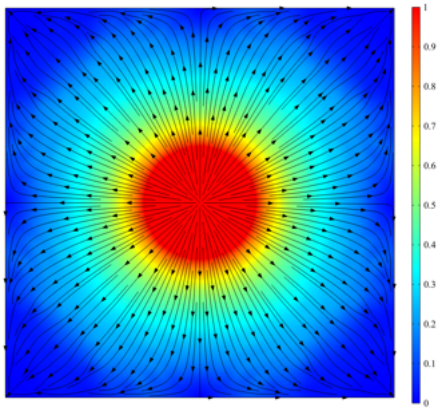

(f) Irrotational intensity field at 1000 Hz

Fig. 4. Structural intensity field and irrotational intensity field distributions in the plate: the color scale indicates the magnitude, and the streamlines indicate the direction of propagation.

The elementary power flow in Fig. 5 represents the flow through each finite element of the section ($x = 0.6\,\mathrm{m}$) calculated using Eq.(7) and Eq.(19). In this particular case the normal to the surface ($x = 0.6\,\mathrm{m}$) is $\mathbf{x}$.

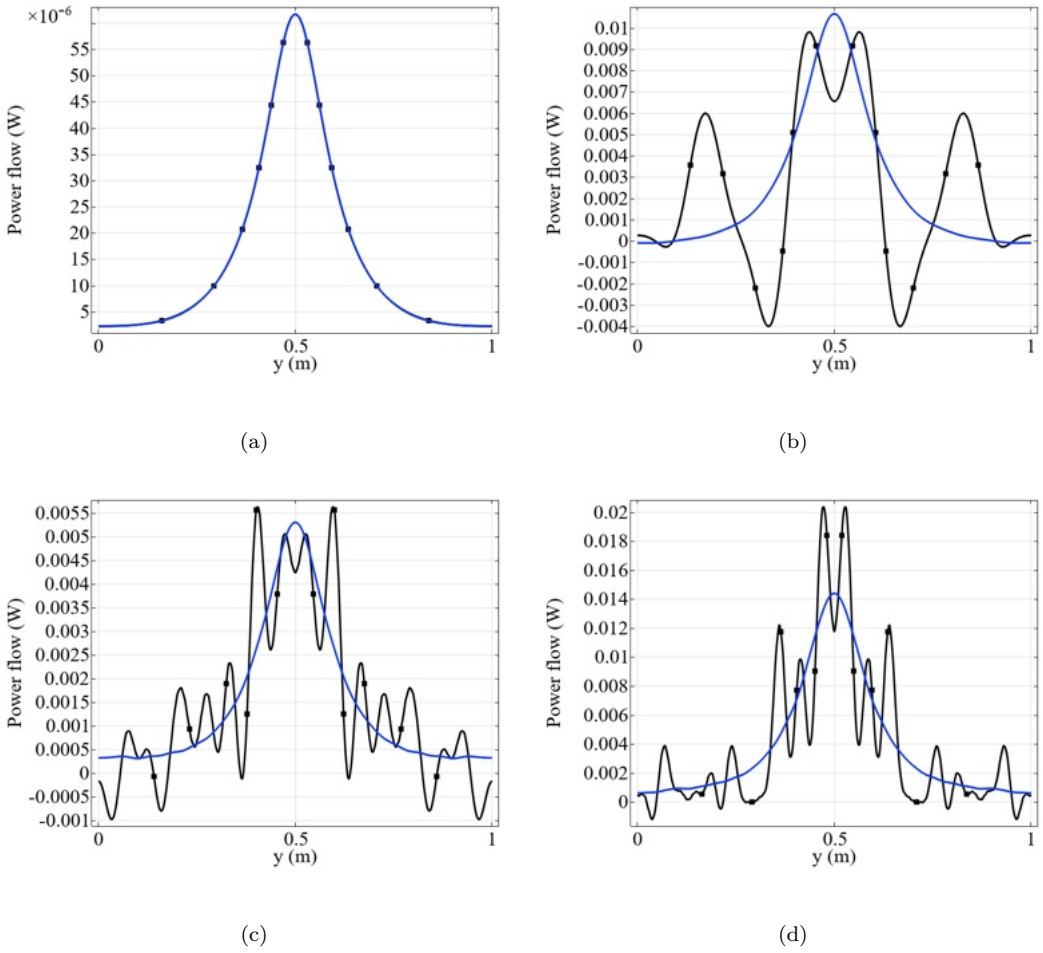

Fig. 5. Elementary power flow through section ($x = 0.6\,\mathrm{m}$) at different frequencies obtained by the structural intensity and the irrotational intensity. (a) 10 Hz; (b) 200 Hz; (c) 1000 Hz; (d) 1500 Hz; (●) Structural intensity;(—) Irrotational intensity.

At very low frequencies, the power flows across the section obtained using the irrotational and structural intensity are identical. This confirms the irrotational behavior of the structural intensity field in this frequency range. At medium and high frequencies, the flow obtained with the irrotational intensity spatially smooths the total structural intensity, additionally pro-

viding frequency-independent information. Therefore, it is highly preferable to use the irrotational intensity for a safe analysis of vibration propagation at mid and high frequencies. Indeed, in this first simple case the intensity pattern provides an understandable way to analyze the system, regardless of the frequency.

5. POWER FLOW ANALYSIS USING THE IRROTATIONAL INTENSITY FIELD IN A PLATES ASSEMBLY

To illustrate the ability of the irrotational intensity field to properly describe the energy transfer path in assembled structures, a four rectangular plates assembly is considered. This structure has the same properties as the previous plate (see Table 1). It is simply supported on its sides. It is excited by a harmonic normal force of 1 N on plate 1, and a viscous damper of $30\,\mathrm{N\,m\,s^{-1}}$ is located on plate 4 as shown in Fig. 6. To ensure convergence at high frequencies, a uniform and fine mesh has been employed, consisting of linear quadrilateral elements of size 0.02×0.02.

Fig. 6. Simply supported structure made with assembled plates

Fig. 7 presents the structural intensity field and the associated irrotational intensity field at different frequencies. Again, in the following, intensity fields and power flow are presented for a unit power input. The color describes the magnitude of the vibration energy in the structure. The structural intensity field is complex and difficult to understand. It provides more information than needed since the primary objective is to know how the vibration energy propagates from one plate to another. The irrotational intensity field shows an average distribution of the vibration energy propagation. This allows us to perfectly localize the position of the source on plate 1 and the sink due

to the viscous damper on plate 4. The power flow is also clearly visible: the energy transfer path is distributed similarly between plates 2 and 3. The dissipation of vibration energy is represented by the color change of the irrotational intensity field.

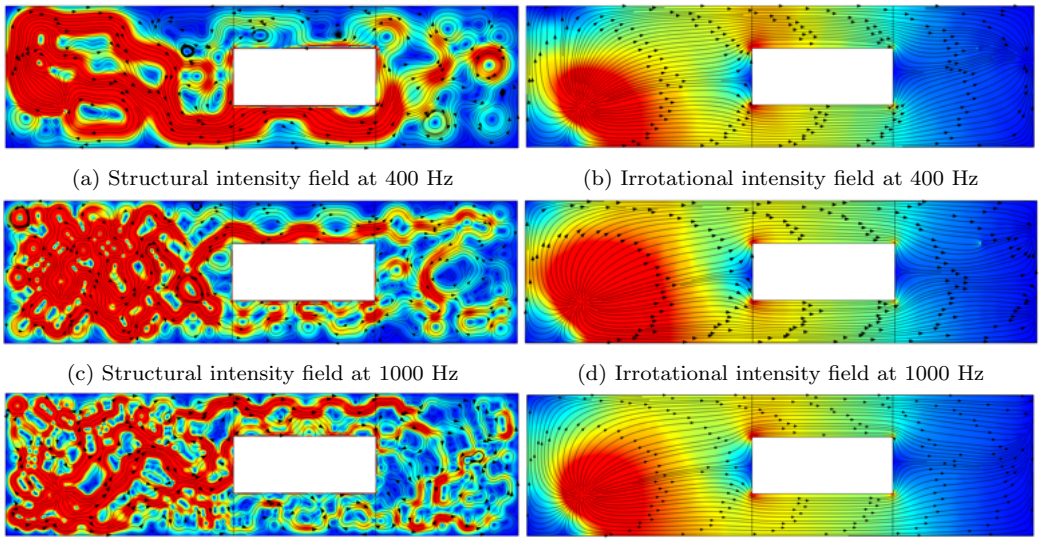

(a) Structural intensity field at 400 Hz (b) Irrotational intensity field at 400 Hz

(c) Structural intensity field at 1000 Hz (d) Irrotational intensity field at 1000 Hz

(e) Structural intensity field at 2000 Hz (f) Irrotational intensity field at 2000 Hz

Fig. 7. Structural intensity field and irrotational intensity field distributions. The color indicates the field magnitude; the streamlines indicate the direction of propagation.

A modification is then introduced to the structure to investigate the influence of damping heterogeneity on the path of vibration energy. The structural damping is no longer homogeneous over the entire structure. A damping of 3% is introduced on plate 3, while the other plates maintain the 1% damping, as shown in figure 8.

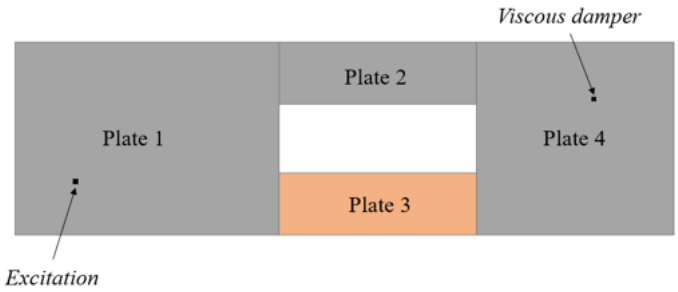

Fig. 8. Simply supported structure with heterogeneous structural damping

Fig. 9 shows the corresponding intensity fields. The propagation of vibration energy is no longer symmetric. The irrotational intensity plot clearly shows that more energy flows through plate 2 than through plate 3. As expected, more power is dissipated in plate 3 due to the increase in structural damping.

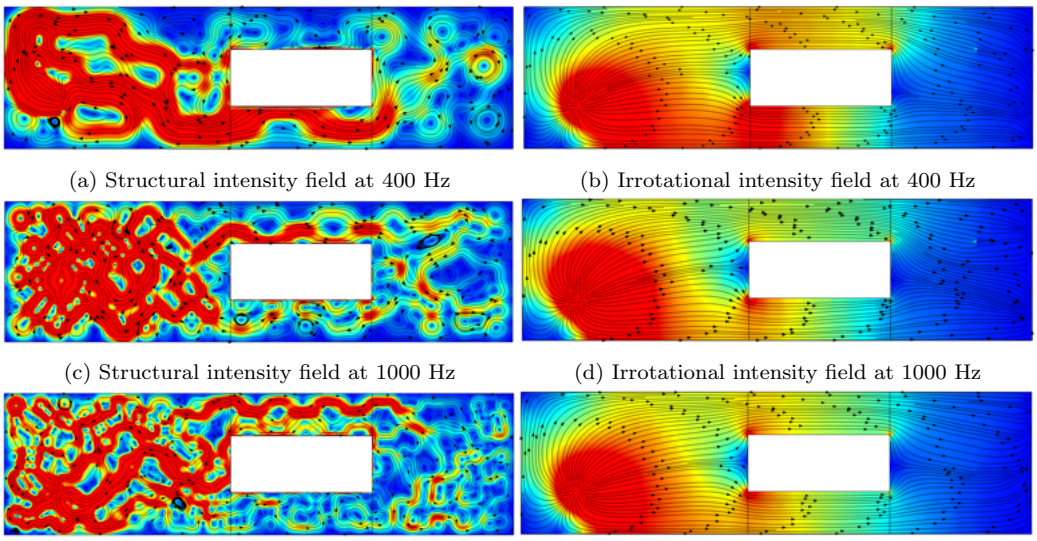

(a) Structural intensity field at 400 Hz

(b) Irrotational intensity field at 400 Hz

(c) Structural intensity field at 1000 Hz

(d) Irrotational intensity field at 1000 Hz

(e) Structural intensity field at 2000 Hz

(f) Irrotational intensity field at 2000 Hz

Fig. 9. Structural intensity field and irrotational intensity field distributions in heterogeneous plate. The color indicates the field magnitude; the streamlines indicate the direction of propagation.

Table 2 shows the injected power obtained in the two configurations: structure with homogeneous structural damping (configuration 1) and structure with heterogeneous structural damping (configuration 2). Notably, the

power input is slightly different between the two configurations. This highlights the robustness of the structural input mobility to damping changes. Tables 3 and 4 compare the net power exchanged between connected plates in both configurations.

The total power flow is calculated using the full field of the structural intensity Eq.(18). The irrotational and rotational power flows are computed using Eq.(19) and Eq.(20) respectively.

Frequency (Hz)	Injected power in configuration 1 (W)	Injected power in configuration 2 (W)
400	5.87×10^{-5}	6.44×10^{-5}
1000	3.95×10^{-4}	4.00×10^{-4}
2000	1.53×10^{-4}	1.56×10^{-4}

Table 2: Injected power for each frequency in both configurations. Configuration 1: structure with homogeneous structural damping; Configuration 2: structure with heterogeneous structural damping.

Tables 3 and 4 clearly show that, regardless of the frequency, the expected balanced transmission from plate 1 to plates 2 and 3 and from plates 2 and 3 to plate 4 is only revealed by the irrotational power flow. Total power flows, to the contrary, present erratic results that totally defy any analysis.

These results differ because of a global vortex that extends over the 4 plates that can be clearly observed in the structural intensity field at 150 Hz (Fig.9a). Such a vortex induces local power flows that cancel each other at the full system level. Tables 3 and 4 show the difference in the power flows between the plates, which qualifies the vortex behavior. Indeed, a constant power is exchanged between subsystems in a circular manner. Consequently, the energy balance of each plate is preserved in both cases; calculations by structural intensity and calculation by irrotational intensity remain identical.

This last result shows that computing power flows in assembled structures are also biased by the rotational components of the structural intensity at the system level. The analysis of the differences between configurations 1 and 2 now seems more relevant. The irrotational power flows show a logical transmission mostly through plate 2 at all frequencies. In contrast, the total power flow provides an unstable transmission scheme. To properly understand the energy transfer path and correct estimation of power flows, the irrotational intensity must be calculated. The method proposed here is a simple way to reach this goal.

Frequency (Hz)	Total power flow			
	$P_{1\to2}$	$P_{1\to3}$	$P_{2\to4}$	$P_{3\to4}$
400	-0.04	0.40	-0.15	0.32
1000	0.18	0.03	0.15	-0.02
2000	0.25	0.09	0.16	0.03
Frequency (Hz)	Irrotational power flow			
	$P_{1\to2}$	$P_{1\to3}$	$P_{2\to4}$	$P_{3\to4}$
400	0.19	0.17	0.08	0.09
1000	0.10	0.11	0.07	0.06
2000	0.18	0.16	0.09	0.10
Frequency (Hz)	Rotational power flow			
	$P_{1\to2}$	$P_{1\to3}$	$P_{2\to4}$	$P_{3\to4}$
400	-0.23	0.23	-0.23	0.23
1000	0.08	-0.08	0.08	-0.08
2000	0.07	-0.07	0.07	-0.07

Table 3: Normalized power exchanged between the plates in configuration 1: structure with homogeneous structural damping. $P_{i\to}j$ is the power exchanged between plates i and j.

6. Conclusion

The irrotational intensity field is used to investigate the vibration energy transfer. The derivation of the irrotational intensity is performed by solving a simplified equation similar to the thermal conduction equation. The approach involves two steps: the first step consists of studying the frequency response of the structure and calculating the injected power and the dissipated power per unit area; the second step is to solve the diffusion equation using the finite element method thermal solver.

The interest in using the irrotational intensity field is illustrated by two examples: a simple plate and a four-plate assembly. The field shows the spatial average of the real energy flux in the structures. It enables the visualization of the energy paths without the masking effects of energy loops, which are associated with the rotational intensity. The irrotational intensity also serves to precisely quantify the exchange of vibration energy between plates in the case of the plate assembly. Indeed, the calculation of the power

Frequency (Hz)	Total power flow			
	$P_{1\to2}$	$P_{1\to3}$	$P_{2\to4}$	$P_{3\to4}$
400	0.02	0.41	−0.07	0.21
1000	0.19	0.07	0.15	−0.04
2000	0.25	0.11	0.17	−0.01
Frequency (Hz)	Irrotational power flow			
	$P_{1\to2}$	$P_{1\to3}$	$P_{2\to4}$	$P_{3\to4}$
400	0.19	0.24	0.10	0.04
1000	0.11	0.15	0.07	0.04
2000	0.17	0.19	0.09	0.07
Frequency (Hz)	Rotational power flow			
	$P_{1\to2}$	$P_{1\to3}$	$P_{2\to4}$	$P_{3\to4}$
400	−0.17	0.17	−0.17	0.17
1000	0.08	−0.08	0.08	−0.08
2000	0.08	−0.08	0.08	−0.08

Table 4: Normalized power exchanged between the plates in configuration 2: structure with heterogeneous structural damping. $P_{i\to j}$ is the power exchanged between plates i and j.

exchange is prone to error due to the vortices in the flow, which are caused by the rotational intensity.

The irrotational intensity provides a better understanding of the propagation of vibrations, and it is shown that this quantity can perfectly characterize the energy sources and sinks in the plates. The irrotational intensity hence constitutes a valuable tool for the design of complex structures. It easily provides a representation and interpretation of the energy transfer paths in built-up structures and quantifies the energy exchanges between the substructures.

Acknowledgement

This work is supported by Stellantis Group framework, the French ANRT and the Morrocan CNRST, under the joint France-Morocco CIFRE program,

in the context of EIPHI Graduate school (contract ANR-17- EURE-0002).

Appendix A. Divergence of the structural and of the irrotational intensity fields

As shown by Eq.(6) and Eq.(16), both the structural and irrotational intensity fields have the same divergence. The divergence of the structural intensity is required to obtain the irrotational intensity, while a very mode-rich basis in the modal space is necessary to evaluate the structural intensity [23]. This is the reason why the local power balance has been selected to compute the divergence of the structural intensity, since the latter converges faster. Fig.A.10 shows both the divergence of structural intensity and the divergence of the irrotational intensity. The results are obtained using finite differences on the structural and irrotational intensity fields. The white region corresponds to the source, corresponding to a positive divergence due to the injection of power into the structure at this location. On the other hand, the dark regions correspond to areas where vibrational energy is dissipated, resulting in a negative divergence. It is worth noting that the divergence of the structural intensity is less accurate near the source, with the white spot appearing larger than expected as the power is injected at a single node. Thus, the divergence of irrotational intensity exhibits a notably improved convergence, especially in the vicinity of the source.

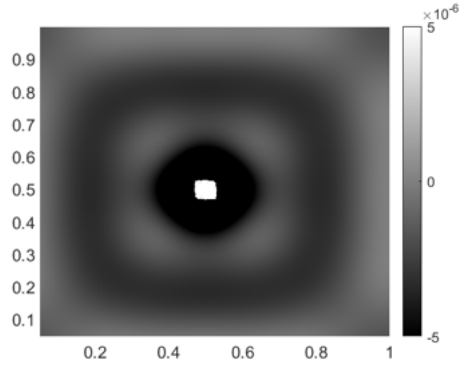

(a) Divergence of the structural intensity field at 200 Hz

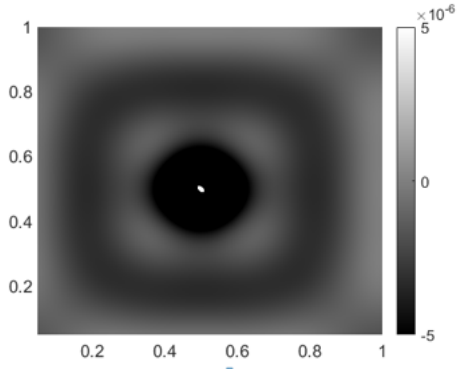

(b) Divergence of the irrotational intensity field at 200 Hz

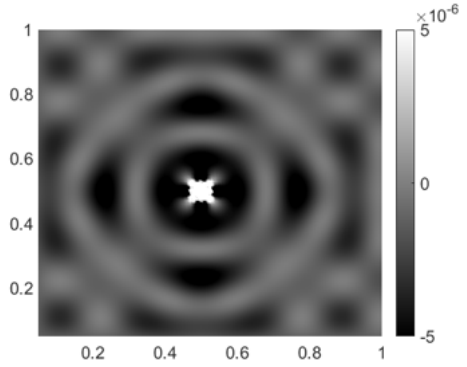

(c) Divergence of the structural intensity field at 1000 Hz

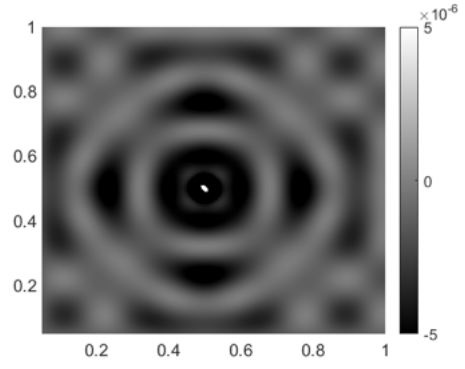

(d) Divergence of the irrotational intensity field at 1000 Hz

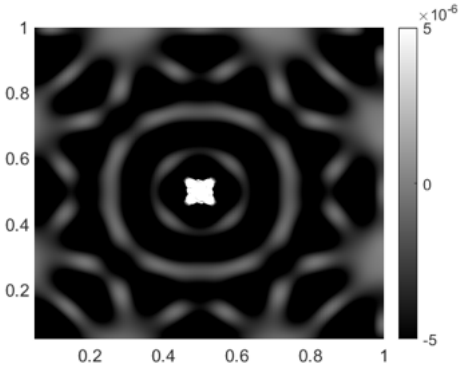

(e) Divergence of the structural intensity field at 1500 Hz

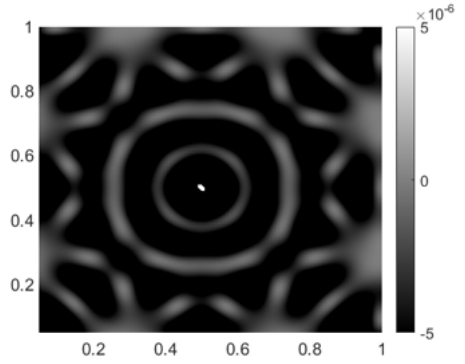

(f) Divergence of the irrotational intensity field at 1500 Hz

Fig. A.10. Structural intensity field and irrotational intensity Divergence.

Appendix B. The irrotational intensity for low structural damping

In order to evaluate the effectiveness of the method for low structural damping, the results of the methodology applied for a case with structural damping of 0.01% are shown here. By decreasing the overall damping, the overall response of the structure remains qualitatively unchanged but the power injected into the structure decreases. As a result, the vibration energy propagation paths generally retain the same configuration as those observed with 1% damping. However, The way in which the energy dissipates in the structure differs, and the amount absorbed by the viscous damping increases due to lower structural damping. The energy now takes longer to dissipate in the structure. It can be seen that the power flows from 1 to 2 and from 1 to 3 are greater than in the previous case (1% structural damping). Similarly, there is also an increase in the flux from 2 to 4 and from 3 to 4.

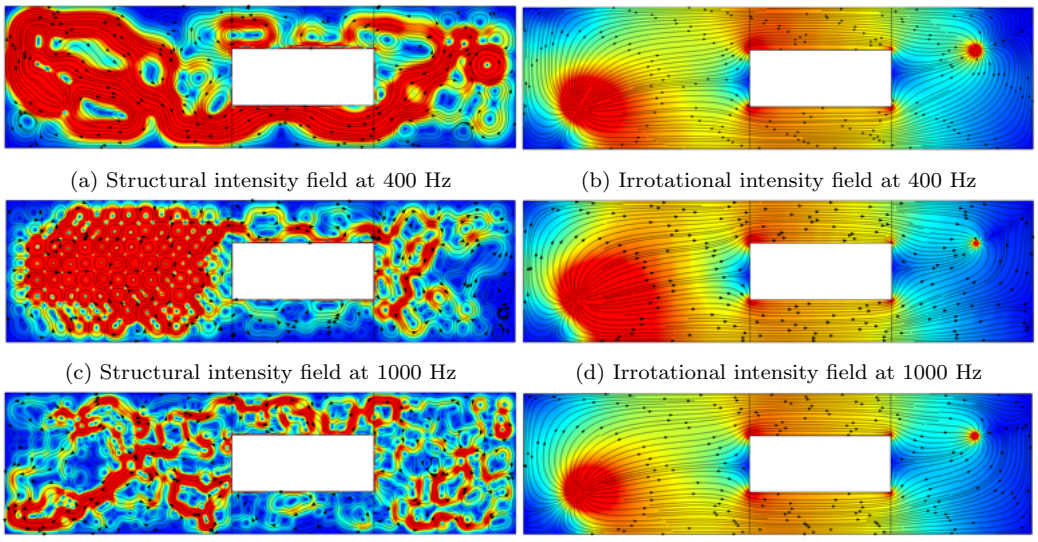

(a) Structural intensity field at 400 Hz

(b) Irrotational intensity field at 400 Hz

(c) Structural intensity field at 1000 Hz

(d) Irrotational intensity field at 1000 Hz

(e) Structural intensity field at 2000 Hz

(f) Irrotational intensity field at 2000 Hz

Fig. B.11. Structural intensity field and irrotational intensity field distributions for low structural damping. The color indicates the field magnitude; the streamlines indicate the direction of propagation.

Frequency (Hz)	Total power flow			
	$P_{1\to2}$	$P_{1\to3}$	$P_{2\to4}$	$P_{3\to4}$
400	-0.05	0.54	-0.12	0.50
1000	0.35	0.16	0.27	0.10
2000	0.58	0.02	0.50	-0.06
Frequency (Hz)	Irrotational power flow			
	$P_{1\to2}$	$P_{1\to3}$	$P_{2\to4}$	$P_{3\to4}$
400	0.25	0.24	0.18	0.20
1000	0.24	0.25	0.16	0.20
2000	0.30	0.30	0.22	0.22
Frequency (Hz)	Rotational power flow			
	$P_{1\to2}$	$P_{1\to3}$	$P_{2\to4}$	$P_{3\to4}$
400	-0.30	0.30	-0.30	0.30
1000	0.11	-0.10	0.11	-0.10
2000	0.28	-0.28	0.28	-0.28

Table B.5: Normalized power exchanged between the plates in configuration 2: structure with heterogeneous structural damping. $P_{i\to j}$ is the power exchanged between plates i and j.

References

[1] R. H. Lyon, Statistical Energy Analysis of Dynamical Systems, MIT Press, Cambridge, Massachusetts, 1975.

[2] A. Le Bot, V. Cotoni, Validity diagrams of statistical energy analysis, Journal of Sound and Vibration 329 (2010) 221–235.

[3] B. M. Gibbs, C. L. S. Gilford, The use of power flow methods for the assessment of sound transmission in building structures, Journal of Sound and Vibration 49 (1976) 267–286.

[4] R. J. Pinnington, R. G. White, Power flow through machine isolators to resonant and non-resonant beams, Journal of Sound and Vibration 75 (1981) 179–197.

[5] R. J. Pinnington, Vibrational power transmission to a seating of a vibration isolated motor, Journal of Sound and Vibration 118 (1987) 515–530.

[6] L. Maxit, J. L. Guyader, Extension of sea model to subsystems with non-uniform modal energy distribution, Journal of sound and vibration 265 (2) (2003) 337–358.

[7] L. Maxit, K. Ege, N. Totaro, J. L. Guyader, Non resonant transmission modelling with statistical modal energy distribution analysis, Journal of Sound and Vibration 333 (2) (2014) 499–519.

[8] H. D. Hwang, L. Maxit, K. Ege, Y. Gerges, J. L. Guyader, Smeda vibro-acoustic modelling in the mid-frequency range including the effect of dissipative treatments, Journal of Sound and Vibration 393 (2017) 187–215.

[9] K. L. Van Buren, M. Ouisse, S. Cogan, E. Sadoulet-Reboul, L. Maxit, Effect of model-form definition on uncertainty quantification in coupled models of mid-frequency range simulations, Mechanical Systems and Signal Processing 93 (2017) 351–367.

[10] G. Zhu, L. Maxit, N. Totaro, A. Le Bot, A hybrid modal/statistical formulation for predicting the energy response of vibroacoustic systems in the mid frequency range, Journal of Sound and Vibration 538 (2022) 117221.

[11] V. Tyrode, Diffuse field assumption for statistical energy analysis: case of coupled non-ergodic billiards, Ph.D. thesis, Ecole Centrale de Lyon (2022).

[12] D. J. Nefdske, S. H. Sung, Power fow finite element analysis of dynamics systems: basic theory and application to beams, Statistical Energy Analysis, ASME Publication NCA-3 (1987) 277–279.

[13] O. M. Bouthier, R. J. Bernhard, Simple models of the energetics of transversely vibrating plates, Journal of Sound and Vibration 182 (1995) 149–164.

[14] R. S. Langley, On the vibrational conductivity approach to high frequency dynamics for two-dimensional structural components, Journal of Sound and Vibration 182 (1995) 637–657.

[15] D. U. Noiseux, Measurement of power flow in uniform beams and plates, Acoustical Society of America 47 (1B) (1970) 238–247.

[16] G. Pavic, Measurement of structure borne wave intensity, part 1: formulation of the methods, Journal of Sound and Vibration 49 (1976) 221–230.

[17] J. C. Pascal, T. Loyau, J. A. Mann, Structural intensity from spatial fourier transformation and bahim acoustical holography method, in: Proceedings of the Structural Intensity and Vibrational Energy Flow, Senlis, France, 1990.

[18] J. R. F. Arruda, P. Mas, Localizing energy sources and sinks in plates using power flow maps computed fom laser vibrometer measurements, Shock and Vibration 5 (1998) 235–253.

[19] J. C. Pascal, X. Carniel, V. Chalvidan, P. Smigielski, Determination of phase and magnitude of vibration for energy flow measurements in a plate using holographic interferometry, Optics and Lasers in Engineering 25 (1996) 343–360.

[20] T. Eck, S. J. Walsh, Measurement of vibrational energy flow in a plate with high energy flow boundary crossing using electronic speckle pattern interferometry, Applied Acoustics 73 (2012) 936–951.

[21] S. Farhadi, H. R. Anani, Reconstruction of vibratory field and structural intensity of vibrating plates using moving sensors, International Journal of Mechanical Sciences 219 (2022) 107059.

[22] S. A. Hambric, Power flow and mechanical intensity calculations in structural finite element analysis, Journal of Vibration and Acoustics 112 (1990) 542–549.

[23] L. Gavric, G. Pavic, A finite element method for computation of structural intensity by the normal mode approach, Journal of Sound and Vibration 164 (1993) 29–43.

[24] X. D. Xu, H. P. Lee, Y. Y. Wang, C. Lu, The energy flow analysis in stiffened plates of marine structures, Thin-Walled Structures 42 (7) (2004) 979–994.

[25] D. Kong, X. Zhang, B. Lu, C. Li, Y. Liu, Identifying dominant components of vibrational energy flow in u-rib plates of bridge based on

structural intensity, Journal of Low Frequency Noise, Vibration and Active Control 0 (2022) 1–17.

[26] L. Wang, T. Chen, Structural intensity analysis of the cantilevered plate under thermal load, Thin-Walled Structures 139 (2019) 209–218.

[27] Y. Wang, J. Du, L. Cheng, Power flow and structural intensity analyses of acoustic black hole beams, Mechanical Systems and Signal Processing 131 (2019) 538–553.

[28] D. S. Cho, K. S. Kim, B. H. Kim, Structural intensity analysis of a large container carrier under harmonic excitations of propulsion system, International Journal of Naval Architecture and Ocean Engineering 2 (2010) 87–95.

[29] D. S. Cho, T. M. Choi, J. H. Kim, N. Vladimir, Structural intensity analysis of stepped thickness rectangular plates utilizing the finite element method, Thin-walled structures 109 (2016) 1–12.

[30] G. Petrone, M. De Vendittis, S. De Rosa, F. Franco, Numerical and experimental investigations on structural intensity in plates, Composite Structures 140 (2016) 94–105.

[31] D. S. Cho, T. M. Choi, J. H. Kim, N. Vladimir, Dominant components of vibrational energy flow in stiffened panels analysed by the structural intensity technique, International Journal of Naval Architecture and Ocean Engineering 10 (5) (2018) 583–595.

[32] P. J. Capasso, G. Petrone, N. Kleinfeller, S. De Rosa, C. Adams, Modeling of fiber composite structures for the calculation of the structural intensity, Composite Structures 262 (2021) 113631.

[33] C. Zhu, J. Yang, Vibration transmission and energy flow analysis of variable stiffness laminated composite plates, Thin-Walled Structures 180 (2022) 109927.

[34] C. Zhu, G. Li, S. Ruan, J. Yang, Structural intensity of laminated composite plates subjected to distributed force excitation, Journal of Vibration Engineering & Technologies (2023) 1–13.

[35] J. C. Pascal, Expressions simplifiées du flux d'énergie dans les plaques, Le Journal de Physique IV 2 (C1) (1992) C1–515.

[36] J. C. Pascal, J. F. Li, Irrotational acoustic intensity: A new method for location of sound sources, in: Proceedings of the sixth international Congress on Sound and Vibration, Copenhagen, Denmark, 1999.

[37] N. B. Roozen, J. L. Guyader, C. Glorieux, H. Muellner, Using the irrotational part of the structural intensity to identify sources of vibrational energy, in: Proceedings of the 22^{nd} International Congress on Acoustics ICA, Buenos Aires, Argentina, 2016.

[38] G. Pavic, Structural surface intensity: an alternative approach in vibration analysis and diagnosis, Journal of Sound and Vibration 115 (1987) 405–422.

[39] G. Pavic, The role of damping on energy and power in vibrating systems, Journal of Sound and Vibration 281 (2005) 45–71.

[40] W. V. D. Hodge, The theory and applications of harmonic integrals, CUP Archive, 1989.

[41] A. Lemoine, J. P. Caltagirone, M. Azaïez, S. Vincent, Discrete helmholtz–hodge decomposition on polyhedral meshes using compatible discrete operators, Journal of Scientific Computing 65 (2015) 34–53.

[42] H. Bhatia, G. Norgard, V. Pascucci, P. T. Bremer, The helmholtz-hodge decomposition—a survey, IEEE Transactions on visualization and computer graphics 19 (8) (2012) 1386–1404.

[43] H. Bhatia, V. Pascucci, P. T. Bremer, The natural helmholtz-hodge decomposition for open-boundary flow analysis, IEEE transactions on visualization and computer graphics 20 (11) (2014) 1566–1578.